New Mexico Geological Society

Downloaded from: https://nmgs.nmt.edu/publications/guidebooks/51



Magmatic history of the Little Hatchet Mountains, Hidalgo and Grant counties, southwestern New Mexico

Ryan Channell, Nancy J. McMillan, Timothy F. Lawton, Matt Heizler, Richard P. Esser, and Virginia T. McLemore

2000, pp. 141-148. https://doi.org/10.56577/FFC-51.141

in:

Southwest Passage: A trip through the Phanerozoic, Lawton, T. F.; McMillan, N. J.; McLemore, V. T.; [eds.], New Mexico Geological Society 51 st Annual Fall Field Conference Guidebook, 282 p. https://doi.org/10.56577/FFC-51

This is one of many related papers that were included in the 2000 NMGS Fall Field Conference Guidebook.

Annual NMGS Fall Field Conference Guidebooks

Every fall since 1950, the New Mexico Geological Society (NMGS) has held an annual Fall Field Conference that explores some region of New Mexico (or surrounding states). Always well attended, these conferences provide a guidebook to participants. Besides detailed road logs, the guidebooks contain many well written, edited, and peer-reviewed geoscience papers. These books have set the national standard for geologic guidebooks and are an essential geologic reference for anyone working in or around New Mexico.

Free Downloads

NMGS has decided to make peer-reviewed papers from our Fall Field Conference guidebooks available for free download. This is in keeping with our mission of promoting interest, research, and cooperation regarding geology in New Mexico. However, guidebook sales represent a significant proportion of our operating budget. Therefore, only *research papers* are available for download. *Road logs*, *mini-papers*, and other selected content are available only in print for recent guidebooks.

Copyright Information

Publications of the New Mexico Geological Society, printed and electronic, are protected by the copyright laws of the United States. No material from the NMGS website, or printed and electronic publications, may be reprinted or redistributed without NMGS permission. Contact us for permission to reprint portions of any of our publications.

One printed copy of any materials from the NMGS website or our print and electronic publications may be made for individual use without our permission. Teachers and students may make unlimited copies for educational use. Any other use of these materials requires explicit permission.

This page is intentionally left blank to maintain order of facing pages.

MAGMATIC HISTORY OF THE LITTLE HATCHET MOUNTAINS, HIDALGO AND GRANT COUNTIES, SOUTHWESTERN NEW MEXICO

RYAN CHANNELL[1], NANCY J. McMILLAN[1], TIMOTHY F. LAWTON[1], MATT HEIZLER[2], RICHARD P. ESSER[2], and VIRGINIA T. McLEMORE[2]

[1]Department of Geological Sciences, Box 30,001, Dept. 3AB, New Mexico State University, Las Cruces, NM, 88003; rchannel@nmsu.edu; nmcmilla@nmsu.edu; tlawton@nmsu.edu; [2]New Mexico Bureau of Mines and Mineral Resources, New Mexico Institute of Mining and Technology, 801 Leroy Pl., Socorro, NM, 8780; matt@nmt.edu; esser@nmt.edu; ginger@nmt.edu

Abstract—Precambrian(?) to Tertiary rocks in the Little Hatchet Mountains provide information on numerous geologic events that occurred in southwestern New Mexico in the last 600 million years. The Precambrian(?) Hatchet Gap granite in the southern Little Hatchet Mountains has controversial U-Pb alpha dates of 640 and 605 Ma (Zeller, 1965), suggesting that it could be related to a suite of Cambrian–Ordovician alkalic and carbonatitic igneous intrusions in New Mexico rather than to older Proterozoic igneous rocks (~1.1 and 1.4 Ga) in the area. The Hatchet Gap granite is in fault contact with Paleozoic strata, which are overlain by the Jurassic Broken Jug Formation. The Broken Jug Formation, correlative to the lower Bisbee Group, consists of marine and non-marine sedimentary rocks as well as subaerial basalt flows formerly interpreted as mafic Cretaceous–Tertiary plutonic rocks. Numerous Cretaceous–Tertiary plutons of the Sylvanite intrusive complex intrude Bisbee Group rocks as young as the Lower Cretaceous U-Bar Formation. The Sylvanite intrusive complex is interpreted as the subvolcanic equivalent of the 71 Ma andesitic Hidalgo Formation in the northern Little Hatchet Mountains. Sylvanite plutonic rocks are mafic–intermediate in composition (50–65% SiO_2), and have high Al_2O_3 (17–19%) and La/Ta (28–39%), similar to samples from the Hidalgo Formation (Young et al., this volume), supporting this correlation. These geochemical data suggest that the Sylvanite intrusive complex was emplaced in a continental arc above the subducting Farallon plate during the Laramide orogeny. $^{40}Ar/^{39}Ar$ age determinations on biotite and K-feldspar of the Granite Pass granite in the southern part of the range yield a weighted mean age of 32.32 ± 0.17 Ma and confirm its Tertiary age. An $^{40}Ar/^{39}Ar$ age determination on the groundmass of a diorite in the Eureka intrusive complex in the northern part of the range suggests that the Eureka complex is no younger than 35.5 ± 1.7 Ma. Thus, the Eureka complex could represent either a shallower and more quickly cooled phase of the Granite Pass granite or a separate, older intrusion.

INTRODUCTION

The southwestern United States has experienced a prolonged and complex history of subduction, continental rifting, alteration, mineralization, and deformation. The Little Hatchet Mountains in Hidalgo and Grant Counties, southwestern New Mexico (Fig. 1), provide an ideal laboratory for study of the tectonics of the southwest U.S. because magmas penetrated the crust in the Little Hatchet Mountains in four of the major tectonic events. The primary goal of this paper is to present new field, geochemical, and geochronologic data that place these igneous rocks into the tectonic framework of western North America.

IGNEOUS GEOLOGY OF THE LITTLE HATCHET MOUNTAINS

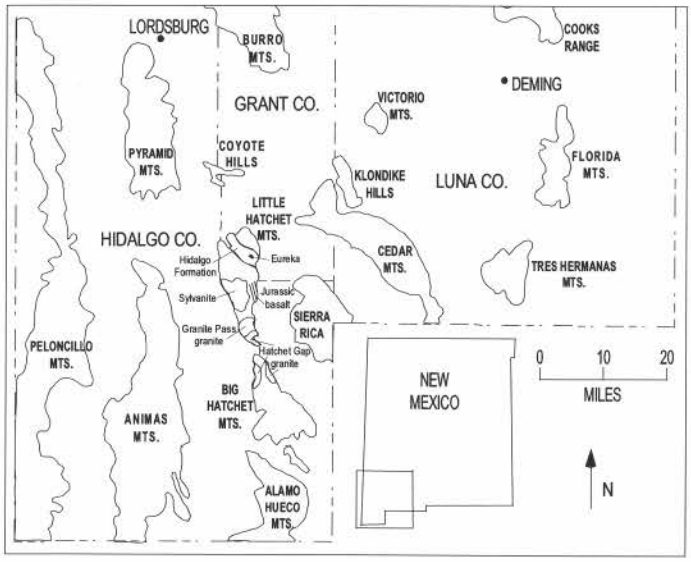
Several suites of igneous rocks, ranging in composition from mafic to silicic and in age from Precambrian(?) to mid-Tertiary, including intrusive and extrusive rock types, are present in the Little Hatchet Mountains. The following sections discuss the field relationships, age determinations, and geochemistry of the suites in chronological order.

Intrusive rocks

A Precambrian(?) granitic pluton, which we designate the Hatchet Gap granite, is located in the southern Little Hatchet Mountains (Fig. 2) and northern Big Hatchet Mountains (Zeller, 1965, 1970, 1975). Zeller (1965) reports lead-alpha ages of 605 and 640 Ma that are consistent with the presence of Upper Cambrian brachiopods in limestone 35 m stratigraphically above the Bliss Sandstone-pluton nonconformity at Hatchet Gap. Although the lead-alpha geochronologic technique has been replaced by more accurate methods, it may provide a rough estimate of the pluton age. For instance, the Granite Pass granite yielded lead-alpha ages of 43 and 48 Ma (Zeller, 1965); new $^{40}Ar/^{39}Ar$ age determinations presented in this paper show that the lead-alpha technique does indeed provide a rough estimate of the actual age of 32.32 ± 0.16 Ma. The Hatchet Gap granite is coarse-grained, porphyritic, and contains plagioclase, microcline, quartz, biotite, and hornblende. Numerous aplite dikes cut the pluton and were assumed to be Precambrian(?) in age because they are also intruded by the mid-Tertiary Granite Pass granite. The Hatchet Gap granite is in fault contact with Pennsylvanian–Permian limestone on its northwest margin and is intruded by the Granite Pass granite on its northern margin.

The Sylvanite intrusive complex (Fig. 2), a network of dioritic–monzonitic intrusions, is located in the central Little Hatchet Mountains near the ghost town of Sylvanite and continues north to the Copper Dick fault. These rocks intruded the Lower Cretaceous Hell-to-Finish and U-Bar formations (Zeller, 1970) as well as the Jurassic Broken Jug Formation (Lawton and Harrigan, 1998), causing pervasive contact metamorphism of the sedimentary units. Zeller (1970) assigned the unit a Cretaceous–Tertiary age. Contacts between the intrusions and sedimentary rocks are sharply defined, but the contacts between the diorite and monzonite are highly variable. The intrusions are generally fine grained with sparse phenocrysts of plagioclase ± Fe-Ti oxides in a groundmass of hornblende + plagioclase ± augite ± K-feldspar ± quartz;

FIGURE 1. Location of the Little Hatchet Mountains in southwestern New Mexico.



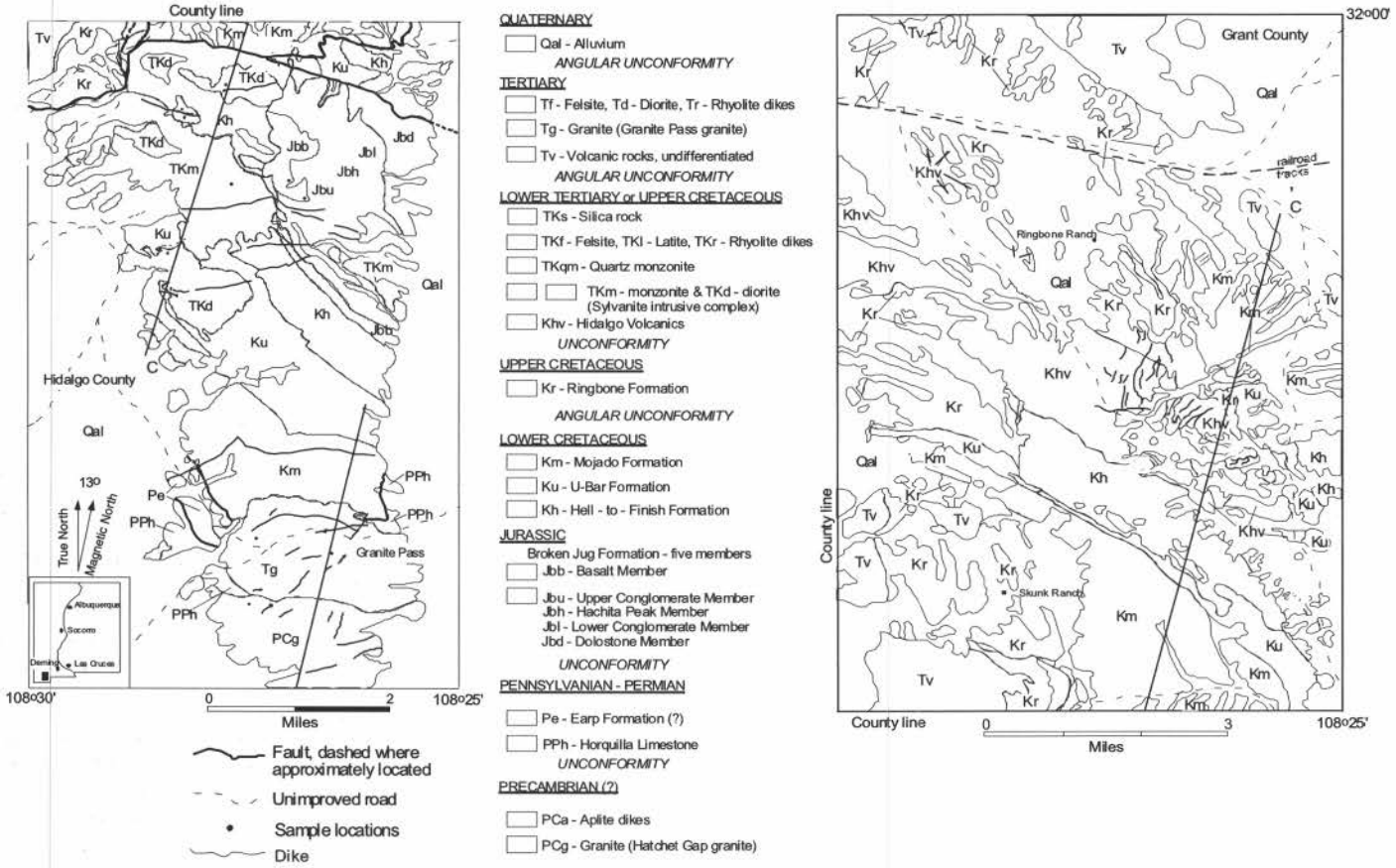


FIGURE 2. Simplified geologic map of the Little Hatchet Mountains. Modified extensively from Zeller (1970). The map on the left depicts the southern half of the range, south of the Hidalgo-Grant County line. The map on the right depicts the northern half of the range, north of the Hidalgo-Grant County line. Note the change in scale between the maps. Straight diagonal lines give the cross-section traverse shown in Figure 7.

diorite is commonly finer-grained than monzonite. Xenoliths of monzonite up to 35 cm diameter are found in the diorite, but intrusive contacts of monzonite into diorite are also found, suggesting that magmas of various compositions intruded the area over a period of time.

The Eureka monzonite-diorite intrusive complex (Old Hachita stock of Zeller, 1970) intruded the volcanic Hidalgo Formation in the northern part of the range (Fig. 1). Zeller (1970) mapped the Eureka stock as Cretaceous–Tertiary in age, which implies that the stock is a shallow intrusive equivalent to the Sylvanite intrusive complex and approximately the same age as the Hidalgo volcanic complex (Young et al., this volume). However, a new $^{40}Ar/^{39}Ar$ age determination on a Eureka diorite presented below yields a mid-Tertiary age for the diorite.

The mid-Tertiary Granite Pass granite intruded Precambrian(?) Hatchet Gap granite, upper Paleozoic limestone, and the Lower Cretaceous Mojado Formation in the southern Little Hatchet Mountains (Fig. 2). East–west- and northeast–southwest-trending dikes of rhyolite and fine grained diorite intruded the pluton. The granite, composed of plagioclase, microcline, quartz, and biotite, is coarse grained and highly weathered.

Volcanic rocks

Volcanic rocks of Late Jurassic(?), Late Cretaceous, and mid-Tertiary age are found in the Little Hatchet Mountains. This study focused on the definition of the Jurassic lava flows and the relationship between Laramide volcanic and plutonic rocks.

Mafic lava flows interbedded with conglomerate, dolostone, and siltstone are present in the east-central part of the range north and south of Broken Jug Pass. The thickness of each lava flow varies from less than 1 m to 30 m. These lavas were mapped as part of the Cretaceous–Tertiary Sylvanite intrusive complex by Zeller (1970); however, the presence of vesicular flow tops and bottoms around massive flow interiors and intercalated sedimentary units precludes a plutonic origin for these rocks. These rocks have been defined as the basalt member of the Upper Jurassic Broken Jug Formation (Lawton and Harrigan, 1998; Lucas and Lawton, this volume) and correlated to basalts in the Bisbee Group in the Chiricahua Mountains of southeast Arizona (Lawton and McMillan, 1999; Lawton and Olmstead, 1995).

The Hidalgo Formation, exposed in the northern Little Hatchet Mountains, is composed of a series of laterally discontinuous and interbedded andesitic autobreccias, heterolithologic breccias, monolithologic breccias, lava flows, dikes, and possibly ash flows along with reworked sedimentary and volcanic detritus (Young et al., this volume). Data presented here and in Young et al. (this volume) suggest that the Hidalgo Formation is the volcanic equivalent of the Sylvanite intrusive complex.

$^{40}Ar/^{39}Ar$ AGE DETERMINATIONS

Biotite and K-feldspar from the Granite Pass pluton and a groundmass concentrate from the Eureka dike were analyzed by incremental heating in a double-vacuum resistance furnace. Analytical methods for argon extraction and mass spectrometry and the isotopic results are listed in Table 1. The Eureka groundmass sample has individual steps with poor precision and overall yields a saddle-shaped spectrum (Fig. 3a; Table 1). The intermediate temperature steps have a weighted mean age of 35.5 ± 1.7 Ma and display minor scatter (MSWD = 3.72) above analytical uncertainty. The K/Ca values are variable, and in general, the higher values correspond to the youngest part of the age spectrum (Fig. 3a).

The biotite age spectrum for the Granite Pass granite is somewhat complex with initial steps yielding anonymously old apparent ages followed by an undulatory spectrum for the remaining heating steps (Fig. 3b). A weighted mean age of 32.54 ± 0.69 Ma is calculated for the final 8 heating steps which comprise 85.4% of the spectrum (Fig. 3b; Table

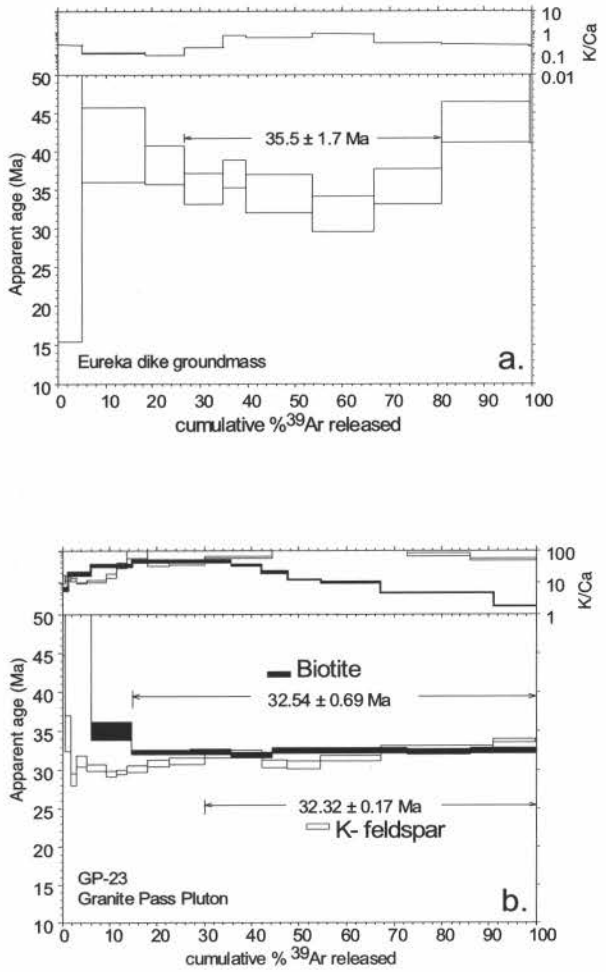


FIGURE 3. $^{40}Ar/^{39}Ar$ incremental heating spectra for Tertiary samples from the Little Hatchet mountains. **A**, Groundmass spectra from the Eureka diorite. **B**, Biotite and K-feldspar spectra from the Granite Pass granite.

1). These steps have a very high MSWD value (43.9; Table 1), which indicates scatter well above that predicted by analytical error alone. The coexisting K-feldspar age spectrum has high apparent ages for initial heating steps that drop to a minimum of ~29 Ma followed by a climb in age to a flat segment for the high-temperature steps (Fig. 3a). The final four heating steps are concordant (MSWD = 2.24) and yield a weighted mean age of 32.32 ± 0.17 Ma (Fig. 3b; Table 1). The K/Ca values are also plotted in Figure 3b and are variable, but typical, for plutonic K-feldspar and biotite.

The weighted mean ages are interpreted to record the time when argon ceased to be lost from each sample. Despite the complexity of the biotite age spectrum from GP-23, the weighted mean age is thought to be geologically relevant in light of the agreement with the weighted mean age given by the coexisting K-feldspar. For rapidly cooled (>10°C/Ma) rocks, the nominal argon-closure temperature for biotite is 350°C (McDougall and Harrison, 1999). K-feldspars have variable argon retentivities (domains) due to their microstructural complexity; however, the high-temperature part of their age spectra generally record cooling below 250–350°C (Lovera et al., 1989). The younger apparent ages of the K-feldspar spectrum record the cooling of the sample through the lower argon retention diffusion domains which typically have closure temperatures of 150–175°C. The concordance of the biotite and K-feldspar ages, coupled with the minor age gradient recorded by the K-feldspar indicates emplacement of the Granite Pass pluton into ambient crustal temperatures of ~200°C. Thus, the combined weighed mean age of the biotite and K-feldspar of 32.33 ± 0.16 Ma is interpreted as the intrusion age of the Granite Pass pluton.

The complexity of the Eureka-groundmass age spectrum does not allow precise age estimation. Saddle-shape age spectra are often indicative of excess argon contamination (Lanphere and Dalrymple, 1976); however, isochron analysis (not shown) does not provide any sensible data array. It is possible that individual phases within the bulk groundmass have slightly variable initial argon concentrations and also that alteration has variably affected the age spectrum. Considering that the minimum part of the age spectrum may be contaminated with excess argon, we suggest that the Eureka dike has a minimum age of 35.5 ± 1.7 Ma.

GEOCHEMISTRY

Whole-rock geochemical data were determined for 32 samples: four Tertiary dikes that intruded the mid-Tertiary Granite Pass granite, four Tertiary(?) dikes that intruded the Sylvanite intrusive complex but are roughly parallel to the Tertiary dikes, 21 diorites and monzonites from the Sylvanite intrusive complex, two samples from the Precambrian(?) Hatchet Gap granite, and one sample of the Granite Pass granite. The Tertiary(?) dikes were mapped by Zeller (1970) as Cretaceous–Tertiary; all other suites conform to his mapped units. Major and trace element analyses by XRF are listed in Table 2; trace elements determined by INAA are listed in Table 3. The major element data are tabulated as analyzed but were normalized to 100% excluding volatiles and with total iron expressed as FeO for plotting and modeling. For comparison, samples from the Laramide Hidalgo Formation (Young et al., this volume), preliminary analyses of basalts of the Broken Jug Formation (Harrigan, 1995), and plutonic rocks from the Florida Mountains intrusion (Ervin, 1998) are plotted on the geochemical diagrams.

The effect of alteration and weathering is apparent on variation diagrams (Fig. 4). Soluble elements such as K_2O, Na_2O, and CaO show wide scatter. Although K_2O is positively correlated with SiO_2, several Sylvanite samples have exceptionally high K_2O concentrations. Two of these samples, LH-076 and LH-014, have low Na_2O as well as high K_2O, suggesting that the alkalis were mobilized during water-rock interaction. Both the Jurassic Broken Jug and Cretaceous Hidalgo volcanic units have low CaO concentrations, suggesting that fluid flow through these permeable units caused more alteration than in the Sylvanite intrusive complex. In contrast, the less soluble elements TiO_2, FeO, MgO, and Y produce good correlations with SiO_2, and can be used to group samples into compositional families and to discern tectonic and magmatic processes.

The Sylvanite samples form linear trends for insoluble elements plotted against SiO_2, suggesting that they are cogenetic (Fig. 4). MgO, FeO, and TiO_2 decrease with increasing SiO_2; Al_2O_3 stays approximately constant. The samples of Hidalgo volcanic rocks plot on trends that almost completely overlap the Sylvanite trend for TiO_2, FeO, MgO, Al_2O_3, and Y; rare earth element (REE) and incompatible trace element concentrations are also similar for the two suites (Fig. 5). The mobile elements Ba, Rb, K, and Sr exhibit significant scatter, but the relatively immobile elements Nb, Ta, Zr, Hf, Ti, and the REE have less scatter. Sylvanite samples have higher overall REE contents and are more strongly light REE-enriched than Hidalgo samples, consistent with the fact that the Sylvanite complex is somewhat more evolved. The two suites share several significant characteristics. Both have positive Eu anomalies, low Ta and Nb (a trough at Ta and Nb on Figure 5, and a Sr peak on Figure 5).

In contrast, preliminary analyses of basalts from the Jurassic Broken Jug Formation (mapped as Sylvanite diorites by Zeller (1970) appear to have compositions that are distinct from Sylvanite magmas. Broken Jug basalts have slightly lower SiO_2 and higher TiO_2 and MgO than Sylvanite plutonic rocks (Fig. 4). Analysis of a complete suite of trace elements for the basalts of the Broken Jug Formation is in progress.

The Precambrian(?) Hatchet Gap granite and the Tertiary Granite Pass granite have similar major element compositions but distinct trace element signatures (Fig. 4). The Hatchet Gap granite has high concentrations of certain trace elements, especially Rb, Zr, and Y. Because this pluton may be Cambrian rather than Precambrian in age, its trace element composition is compared to the Cambrian Florida Mountains intrusion in Figure 6. The Hatchet Gap granite has REE patterns that are

TABLE 1. Isotopic data for $^{40}Ar/^{39}Ar$ age determinations for the Granite Pass granite and the Eureka diorite.

ID	Temp (°C)	$^{40}Ar/^{39}Ar$	$^{37}Ar/^{39}Ar$ (x 10^{-3})	$^{36}Ar/^{39}Ar$ (x 10^{-15} mol)	$^{39}Ar_K$	K/Ca (%)	$^{40}Ar^*$ (%)	^{39}Ar (Ma)	Age (Ma)	±1s
GP-23 K-feldspar, wt. = 16.16 mg, J = 0.0014439, NM-41, Lab # =5825-01										
A	*550*	*5375.6*	-	*17538*	*0.045*	-	*3.6*	*0.0*	*444*	*1964*
B	*550*	*1462.8*	-	*4711*	*0.493*	-	*4.8*	*0.1*	*175*	*74*
C	*650*	*758.2*	-	*2342*	*0.259*	-	*8.7*	*0.1*	*165*	*47*
D	*650*	*216.6*	*0.0404*	*663.5*	*4.00*	*12.6*	*9.5*	*0.7*	*52.7*	*4.0*
E	*750*	*68.84*	*0.0383*	*187.5*	*7.75*	*13.3*	*19.5*	*1.8*	*34.7*	*1.1*
F	*750*	*25.13*	*0.0417*	*47.41*	*8.98*	*12.2*	*44.3*	*3.0*	*28.74*	*0.37*
G	*850*	*24.04*	*0.0548*	*40.57*	*15.3*	*9.3*	*50.1*	*5.2*	*31.12*	*0.33*
H	*950*	*17.57*	*0.0477*	*19.81*	*29.3*	*10.7*	*66.7*	*9.3*	*30.28*	*0.19*
I	*1000*	*13.22*	*0.0323*	*6.079*	*15.6*	*15.8*	*86.4*	*11.5*	*29.53*	*0.15*
J	*1050*	*14.08*	*0.0160*	*8.686*	*15.5*	*31.9*	*81.8*	*13.7*	*29.75*	*0.14*
K	*1150*	*20.01*	*0.0071*	*28.22*	*29.2*	*72.3*	*58.3*	*17.8*	*30.15*	*0.22*
L	*1200*	*19.37*	*0.0137*	*25.11*	*33.8*	*37.2*	*61.7*	*22.6*	*30.85*	*0.20*
M	*1250*	*21.57*	*0.0130*	*32.19*	*52.0*	*39.3*	*55.9*	*29.9*	*31.13*	*0.23*
N	1300	20.83	0.0082	28.69	102.6	62.1	59.3	44.4	31.89	0.19
O	1350	20.27	0.0048	26.02	201.7	105.9	62.1	72.8	32.48	0.18
P	1400	18.99	0.0069	21.85	95.1	74.3	66.0	86.2	32.36	0.16
Q	1750	19.79	0.0098	24.42	98.0	51.8	63.5	100.0	32.47	0.17
total gas age			n = 17			709.5	66.0		32.12	0.41
plateau		MSWD = 2.24	n = 4	steps N–Q	497.3	80.2		70.1	**32.32**	**0.17***
GP-23 Biotite, wt. = 8.0 mg, J = 0.00144353, NM-41, Lab # =5826-01										
A	*600*	*2590.4*	*0.0829*	*8223.1*	*5.27*	*6.2*	*6.2*	*1.3*	*376*	*48*
B	*670*	*432.8*	*0.0277*	*1341.3*	*19.7*	*18.4*	*8.4*	*6.1*	*92.6*	*7.7*
C	740	39.14	0.0154	86.62	35.3	33.1	34.6	14.6	34.94	0.56
D	800	16.10	0.0108	12.16	50.5	47.2	77.7	26.9	32.28	0.14
E	850	16.32	0.0113	12.84	35.7	45.1	76.8	35.5	32.35	0.15
F	900	19.72	0.0149	24.73	27.2	34.3	62.9	42.1	32.03	0.24
G	950	22.68	0.0249	36.39	22.3	20.5	52.6	47.5	30.79	0.27
H	1020	21.18	0.0421	31.54	28.8	12.1	56.0	54.5	30.63	0.26
I	1100	16.32	0.0532	13.99	51.9	9.6	74.7	67.1	31.47	0.14
J	1200	14.17	0.1106	4.874	98.4	4.6	89.9	91.0	32.88	0.10
K	1650	14.40	0.2857	4.389	37.1	1.8	91.1	100.0	33.86	0.11
total gas age			n = 11			412.0	20.2		39.8	1.2
plateau		MSWD=43.9**	n = 8	steps D–K	351.8	19.2		85.4	**32.54**	**0.69***
EUREKA groundmass, wt. = 10.4 mg, J = 0.0014567, NM-41, Lab # =5810-01										
A	*600*	*663.7*	*1.983*	*2191.1*	*3.47*	*0.26*	*2.5*	*5.0*	*43*	*14*
B	*700*	*126.6*	*4.585*	*376.5*	*9.07*	*0.11*	*12.4*	*18.2*	*40.9*	*2.4*
C	775	66.21	5.720	176.0	5.66	0.089	22.1	26.5	38.2	1.2
D	850	52.08	2.627	131.4	5.64	0.19	25.9	34.7	35.1	1.0
E	900	40.52	0.7213	89.09	3.36	0.71	35.2	39.6	37.09	0.88
F	1000	66.43	0.8797	180.2	9.52	0.58	20.0	53.4	34.5	1.2
G	1100	63.19	0.6010	172.5	8.99	0.85	19.4	66.5	31.9	1.1
H	1200	63.24	1.595	168.5	9.84	0.32	21.5	80.8	35.4	1.2
I	*1300*	*76.75*	*1.946*	*203.2*	*12.7*	*0.26*	*22.0*	*99.3*	*43.8*	*1.3*
J	*1400*	*96.01*	*2.292*	*257.4*	*0.449*	*0.22*	*21.0*	*100.0*	*52.2*	*5.6*
total gas age		n = 10			68.7	0.37			37.9	2.0
plateau	MSWD=3.72	n = 6		steps C–H	43.0	0.47		62.6	**35.5**	**1.7***

Notes:
Isotopic ratios corrected for blank, radioactive decay, and mass discrimination, not corrected for interfering reactions.
Individual analyses show analytical error only; total gas and plateau age error includes error in J and irradiation parameters.
n = number of heating steps
K/Ca = molar ratio calculated from reactor-produced ^{39}ArK and $^{37}ArCa$.
Analyses shown in italics not used for plateau age calculation.
- no detectable ^{37}Ar.
2s error
** MSWD outside of 95% confidence window, error multiplied by square root of MSWD.

very similar to the Florida Mountains intrusion (Fig. 6a), including a large negative Eu anomaly and flat heavy REE abundances. Similarly, the two granites are similar in incompatible trace element abundances (Fig. 6b), with a few major exceptions. Both plutons show depletions at Sr, P, and Ti; however, the Little Hatchet Mountains granite shows troughs at Zr and Nb-Ta that are not found in the Florida Mountains intrusion.

DISCUSSION

Igneous rocks in the Little Hatchet Mountains were emplaced during four major tectonic events since late Proterozoic or early Paleozoic time: late Proterozoic–Cambrian(?) magmatism, Late Jurassic rifting, Laramide (Late Cretaceous–Eocene) compression, and mid-Tertiary Basin-and-Range extension. The new age determinations, field relationships, and geochemical data presented in this paper and additional mapping constrain a new north–south cross-section through the Little Hatchet Mountains (Fig. 7). Data on the Hatchet Gap granite and the Eureka stock do not conclusively constrain their role in the tectonic history of the region. The tectonic implications of data for the Jurassic and Cretaceous suites are discussed below.

The discovery of Jurassic basalt flows in the Little Hatchet Mountains

TABLE 2. Major and trace element analyses of igneous rocks from the Little Hatchet Mountains. Oxides are listed in weight percent; elements are listed in parts per million (ppm).

Sample	LH006	LH008	LH002	LH010	LH011	LH012	LH014	LH016	LH017	LH018	LH019	LH020	LH024	LH026	LH028	LH029
Unit	1	1	2	2	2	2	2	2	2	2	2	2	2	2	2	2
SiO_2	74.9	76.2	53.1	58.1	56.9	51.4	55.3	60.6	62.47	63.27	59.14	54.56	55.50	51.56	50.89	52.02
TiO_2	0.15	0.09	1.14	0.77	0.9	1.35	1.01	0.79	0.69	0.51	0.72	0.92	0.90	1.44	1.08	0.98
Al_2O_3	12.1	12.8	17.3	16.2	16.9	17.1	12.2	16.3	16.37	17.41	17.89	18.01	17.14	15.70	16.27	18.18
Fe_2O_3	1.23	0.4	7.25	5.19	7.6	8.38	6.66	4.98	4.38	2.36	2.12	6.87	6.92	10.78	9.21	8.00
MnO	0.02	0	0.08	0.07	0.2	0.05	0.13	0.08	0.08	0.04	0.05	0.16	0.20	0.148	0.11	0.19
MgO	0.17	0.08	3.17	2.62	2.19	3.67	1.37	1.42	1.57	1.05	2.22	2.42	2.07	3.61	4.74	2.79
CaO	0.41	0.09	8.2	5.45	6.38	9.85	11.2	4.34	4.57	4.02	6.54	7.79	6.96	9.48	5.42	8.32
Na_2O	2.98	3.58	4.31	3.66	4.33	3.87	0.44	4.3	4.12	6.46	5.95	3.96	4.57	1.69	2.92	4.17
K_2O	5.85	5.07	2.43	1.73	2.61	1.96	8.8	3.28	3.61	2.18	2.95	2.04	1.92	2.01	6.00	2.30
P_2O_5	0.03	0.01	0.5	0.2	0.39	0.67	0.1	0.33	0.25	0.22	0.41	0.43	0.56	0.41	0.35	0.49
LOI	0.44	0.44	1.85	4.92	1.74	0.78	2.51	2.54	1.24	0.63	1.11	1.87	1.71	2.14	1.27	2.19
TTL	98.29	98.76	99.31	98.94	100.06	99.11	99.61	98.97	99.35	98.15	99.10	99.03	98.45	98.97	98.26	99.63
V	3	4	173	100	136	174	89	76	72	39	89	150	116	275	226	157
Cr	12	6	15	41	10	13	116	18	14	6	23	11	16	76	113	7
Ni	4	2	9	21	6	21	65	7	6	6	8	6	6	34	34	5
Cu	17	4	9	5	6	11	10	13	13	28	23	6	13	6	122	4
Zn	38	16	79	73	100	34	41	36	36	35	88	83	145	111	83	169
Ga	19	16	21	18	22	21	12	20	19	23	21	24	23	20	18	22
As	b/d	6	6	3	6	7	3	3	2	4	6	4	4	3	8	6
Rb	333	149	58	37	74	32	153	64	61	60	71	35	34	51	164	49
Sr	37	26	913	714	431	1221	121	776	732	871	885	1136	915	824	493	758
Y	78	22	21	22	24	25	29	22	19	24	18	24	21	23	20	21
Zr	173	87	171	190	233	161	197	206	218	234	206	225	187	132	119	153
Nb	19	26	9	4	15	7	11	10	9	18	17	17	12	4	4	6
Ba	250	128	864	481	761	1365	1446	1218	1178	555	758	1031	877	891	1570	1063
Pb	23	10	12	7	14	2	3	3	6	9	15	17	16	13	3	15
Th	30	9	7	3	5	4	1	9	12	6	3	6	5	6	6	5
U	6	2	1	1	3	1	3	2	2	2	1	2	1	0	2	1

Sample	LH030	LH032	LH034	LH035	LH036	LH075	LH076	LH001	LH013	LH015	LH025	LH004	LH003	LH005	LH007	LH009
Unit	2	2	2	2	2	2	2	3	3	3	3	4	5	5	5	5
SiO_2	61.31	59.02	47.36	56.52	59.64	50.97	54.05	70.3	77.6	75.9	72.95	76.1	76.6	59	51.9	75.6
TiO_2	0.66	0.81	1.48	0.99	0.98	1.05	1.20	0.34	0.08	0.09	0.15	0.12	0.1	0.86	1.03	0.1
Al_2O_3	16.89	17.27	16.98	16.51	16.62	18.17	17.20	14.6	12.4	12.8	14.39	13.1	12.9	17.1	15.6	13
Fe_2O_3	4.81	5.53	13.87	7.22	2.17	9.12	8.42	1.64	0.69	0.68	1.46	0.41	0.35	5.76	7.09	0.54
MnO	0.10	0.09	0.26	0.16	0.08	0.10	0.13	0.05	0.01	0.03	0.04	0	0.01	0.14	0.1	0.05
MgO	1.29	2.32	7.17	2.93	2.35	2.90	4.58	0.32	0.1	0.11	0.30	0.09	0.07	2.63	4.51	0.11
CaO	5.24	6.15	3.98	6.31	7.92	5.08	6.21	1.15	0.2	0.07	1.33	0.44	0.09	4.79	6.82	0.4
Na_2O	4.62	4.86	4.82	3.79	4.60	2.50	0.95	4.14	4.99	2.92	5.02	3.26	3.93	3.9	3.3	3.95
K_2O	2.39	2.60	0.22	2.03	3.64	4.47	4.81	5.23	2.67	5.53	1.90	5.3	4.7	2.37	2.42	4.6
P_2O_5	0.23	0.43	0.26	0.60	0.45	0.79	0.52	0.05	0.01	0.02	0.08	0.02	0.02	0.23	0.36	0.02
LOI	1.93	0.72	3.30	2.08	1.09	4.88	2.52	1.59	0.66	0.78	1.72	0.51	0.42	2.54	5.16	0.67
TTL	99.47	99.80	99.70	99.14	99.54	100.03	100.59	99.41	99.36	98.88	99.34	99.39	99.12	99.27	98.26	99.08
V	83	68	202	102	63	160	174	9	5	6	9	7	4	98	136	5
Cr	11	25	259	55	20	6	81	5	7	3	5	6	7	24	97	6
Ni	5	9	216	19	7	5	25	5	3	3	3	2	2	14	64	3
Cu	31	6	18	6	9	11	9	3	3	6	21	5	5	3	6	7
Zn	174	59	109	117	49	112	114	32	41	43	35	25	14	161	93	38
Ga	21	22	20	22	21	23	22	17	18	21	16	17	16	20	20	16
As	4	10	2	4	3	4	6	b/d	b/d	b/d	2	1	6	4	2	15
Rb	53	52	3	32	63	121	38	195	110	293	77	207	125	90	70	107
Sr	941	881	322	978	956	926	1236	193	103	40	464	58	28	708	653	55
Y	19	20	24	27	22	27	25	37	36	40	32	28	15	25	30	22
Zr	245	207	102	157	179	174	169	325	115	115	144	67	86	229	226	112
Nb	16	11	10	9	9	10	8	16	41	43	15	25	29	8	9	33
Ba	1159	1376	157	1059	1179	796	416	1044	48	76	634	140	145	673	595	328
Pb	19	9	2	13	4	7	15	17	15	17	22	22	15	25	7	33
Th	12	7	0	5	6	6	5	18	26	28	10	22	2	5	4	11
U	3	2	0	0	3	3	3	3	9	6	2	5	2	1	1	2

b/d = below detection
1 = Precambrian(?) Hatchet Gap granite and associated aplite dikes
2 = Laramide Sylvanite intrusive complex composed of diorite and monzonite
3 = Tertiary(?) dikes cutting the Sylvanite intrusive complex
4 = Tertiary Granite Pass granite
5 = Tertiary dikes cutting Granite Pass granite
XRF analyses performed at the New Mexico Bureau of Mines and Mineral Resources

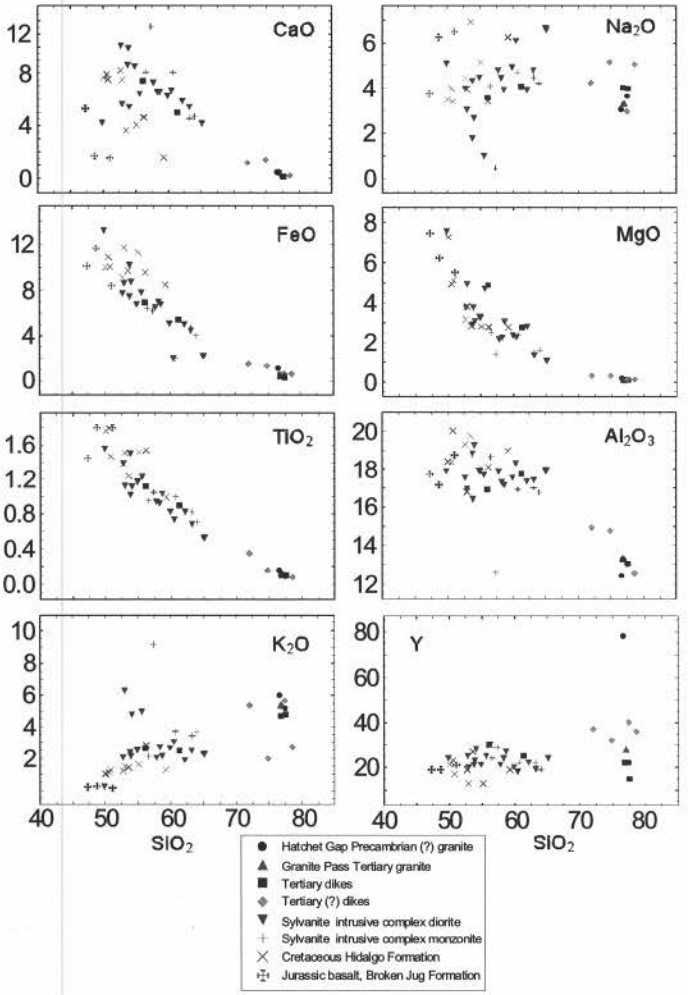


FIGURE 4. SiO_2-variation diagrams for the igneous rocks of the Little Hatchet Mountains.

TABLE 3. INAA trace-element analyses of select igneous rocks from the Little Hatchet Mountains. Data are in ppm.

Sample	LH004	LH006	LH012	LH019	LH034	LH035	LH036
Eu	0.495	0.875	2.897	1.654	1.356	2.470	2.461
Hf	4.11	6.71	4.14	5.45	2.25	4.24	5.07
Ni	b/d	b/d	26	b/d	101	b/d	b/d
Rb	205.7	325.1	34.8	70.5	6.2	35.6	66.1
Sb	0.34	0.31	0.49	0.41	b/d	0.34	0.08
Sc	3.48	2.72	14.44	7.17	26.06	10.89	8.95
Sr	60	28	1373	1008	244	1101	1051
Ta	2.72	2.13	0.74	1.15	0.69	0.89	1.06
Tb	0.66	1.91	0.81	0.57	0.56	0.81	0.75
Th	25.65	33.96	5.05	6.23	0.69	4.48	6.41
Zn	24	45	35	108	94	142	48
Zr	117	165	132	153	129	157	178
As	b/d	b/d	3.4	4.5	b/d	b/d	1.7
Ba	167.2	250.2	1154.0	697.4	196.2	986.8	1087.0
La	12.92	61.17	20.75	28.35	17.52	35.16	38.98
Lu	0.667	1.212	0.297	0.217	0.278	0.305	0.301
Nd	14.25	46.03	30.13	25.76	15.17	33.56	40.45
Sm	4.34	11.21	7.01	5.24	3.77	7.13	6.97
U	8.19	6.82	1.17	1.71	b/d	1.76	3.34
Yb	4.00	8.93	2.22	1.42	2.20	2.20	2.06
Ce	32.9	134.9	49.0	56.0	35.3	73.4	89.8
Co	0.11	1.00	13.80	4.01	54.34	16.25	5.28
Cr	b/d	0.9	7.3	11.5	209.8	39.2	16.
Cs	1.52	1.98	0.55	0.76	0.34	1.77	0.55

b/d = below detection

INAA analyses performed at the Research Reactor Center University of Missouri-Columbia

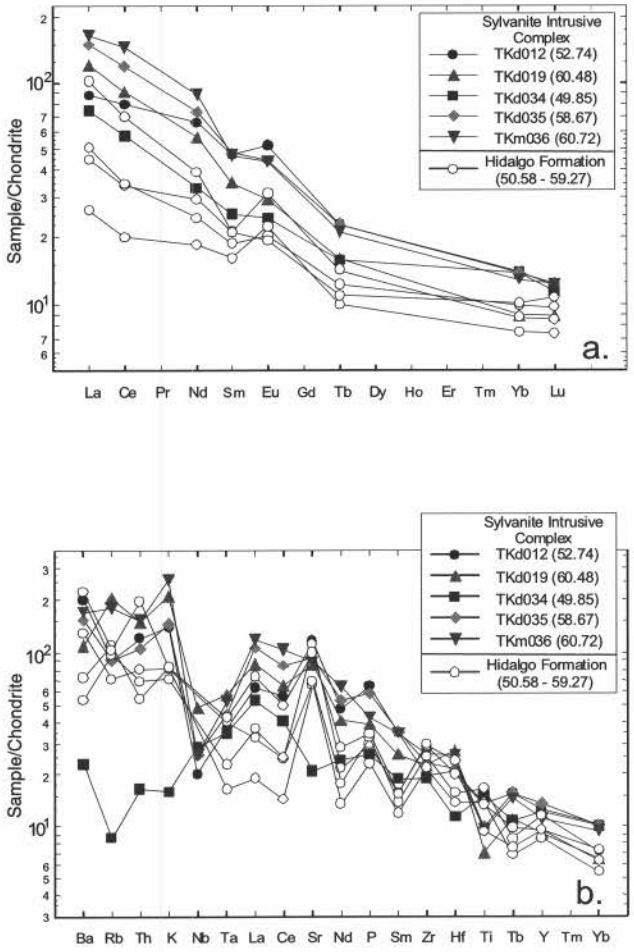


FIGURE 5. **A**, Chondrite-normalized rare-earth-element diagram comparing rocks of the Sylvanite intrusive complex to rocks of the Hidalgo volcanic center (Young et al, this volume), normalized using values of Wasson (1985). **B**, Chondrite-normalized incompatible trace-element diagram for the same suites, using normalization factors of Thompson (1982).

by Harrigan (1995) and the definition of the Jurassic Broken Jug Formation by Lawton and Harrigan (1998) were the first indications that the mafic rocks mapped by Zeller (1970) as Laramide plutons actually included both Laramide plutons of the Sylvanite intrusive complex and Jurassic basalt flows of the Broken Jug Formation. The Broken Jug Formation has been correlated to the Crystal Cave and Onion Saddle formations in the Bisbee Group in the Chiricahua Mountains of Arizona (Lawton and Harrigan, 1998; Lawton and Olmstead, 1995). Preliminary geochemical and petrographic analysis by Harrigan (1995) and Lawton and McMillan (1999) indicates that the Broken Jug basalts are similar in major and trace element composition to the Chiricahua basalts, suggesting that they erupted into Late Jurassic grabens or half-grabens in the Mexican Borderland rift. Major- and trace-element analysis of a complete suite of Broken Jug basalts is in progress.

The mafic–intermediate Sylvanite intrusive complex shares mineralogic, compositional, and geochronologic features with the Hidalgo Formation that suggest that the Sylvanite complex is the subvolcanic pluton that supplied the Hidalgo composite cone. The two suites of rocks exhibit similar major and trace element trends. SiO_2 and incompatible element concentrations extend to higher values in the Sylvanite complex (Figs. 4, 5), suggesting that differentiation continued after volcanism ceased. Although the concentrations of mobile incompatible trace elements Ba, Rb, K, and Sr vary greatly between the two suites, immobile elements such as the REE, Hf, Zr, Nb, and Ta show similar patterns. For instance, both suites have comparable low Ta/La ratios (Hidalgo: 0.035–0.076, Young et al., this volume; Sylvanite:

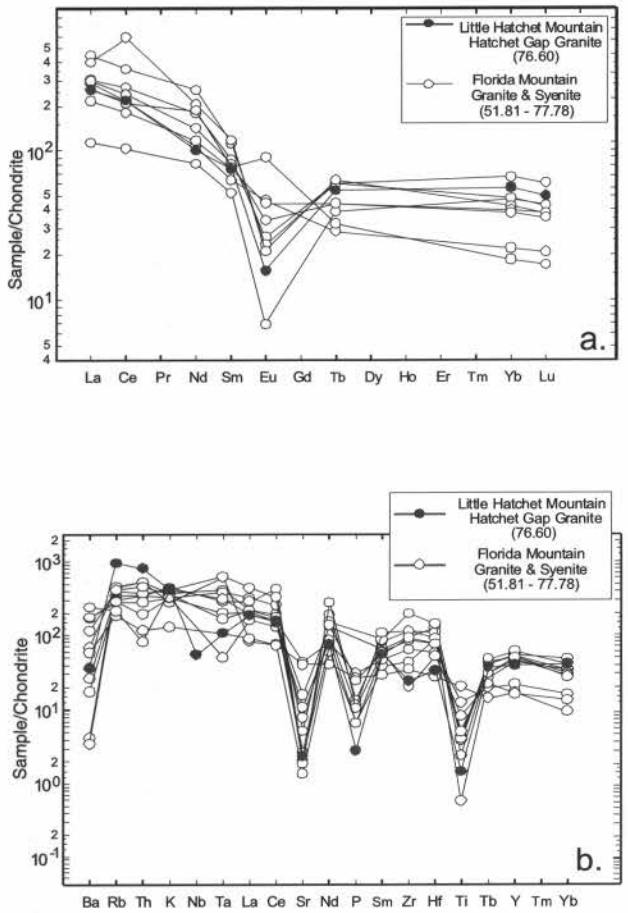


FIGURE 6. **A**, Chondrite-normalized rare-earth-element diagram comparing rocks of the Precambrian(?) granite of the Little Hatchet Mountains to the 511-Ma orthoclase granite of the Florida Mountains (Ervin, 1998). **B**, Chondrite-normalized incompatible-trace-element diagram for the same suites of rocks.

0.025–0.056) and positive Eu anomalies (Fig. 5). Hornblende crystals from Hidalgo volcanic rocks consistently yield $^{40}Ar/^{39}Ar$ ages ~71 Ma (Young et al., this volume); the Sylvanite intrusive complex intruded rocks as young as the Upper Cretaceous U-bar Formation and must post-date them. Thus, it is likely that the Sylvanite intrusive complex and the Hidalgo Formation comprise a Laramide plutonic-volcanic pair that could be used to understand plumbing dynamics of arc volcanoes.

Tertiary age plutonism is currently being investigated, for little is known about the relationship between the Granite Pass granite, the Eureka monzonite stock, and the numerous silicic and intermediate dikes throughout the range. The $^{40}Ar/^{39}Ar$ data suggest that both were emplaced during the Basin-and-Range extension and that at least the mafic rocks associated with the Eureka stock are not part of the Sylvanite intrusive complex. The Granite Pass granite is not associated with structures that suggest that it floored a caldera; thus, we suspect that the ash-flow sheets at and near Playas Peak were erupted from other calderas in the Bootheel volcanic field (McIntosh and Bryan, this volume).

CONCLUSIONS

Magmas were emplaced in the Little Hatchet Mountains area as plutons or volcanic rocks during four major tectonic events since late Proterozoic time. This paper uses field, geochronologic, and geochemical data to place these igneous rocks into the tectonic framework of the evolution of the region. Two of these igneous suites have not been widely recognized in New Mexico geology. Jurassic mafic volcanism during deposition of Bisbee Group sedimentary rocks in the Mexican Borderland rift (Lawton and McMillan, 1999) is recorded as basalt flows in the Broken Jug Formation. The Hatchet Gap granite may be part of a series of alkalic plutons of Cambrian-Ordovician age related to early Paleozoic extension (McMillan et al., this volume).

The Laramide Sylvanite intrusive complex in the central Little Hatchet Mountains is similar in mineralogy, age, and composition to the Hidalgo volcanic complex exposed in the northern part of the range, and probably represents the subvolcanic roots of the Hidalgo composite cone. New age determinations for Cenozoic igneous rocks of the Granite Pass granite and the Eureka stock confirm a mid-Tertiary age; however, these plutons are probably not related to the Tertiary pyroclastic rocks of the Little Hatchet Mountains.

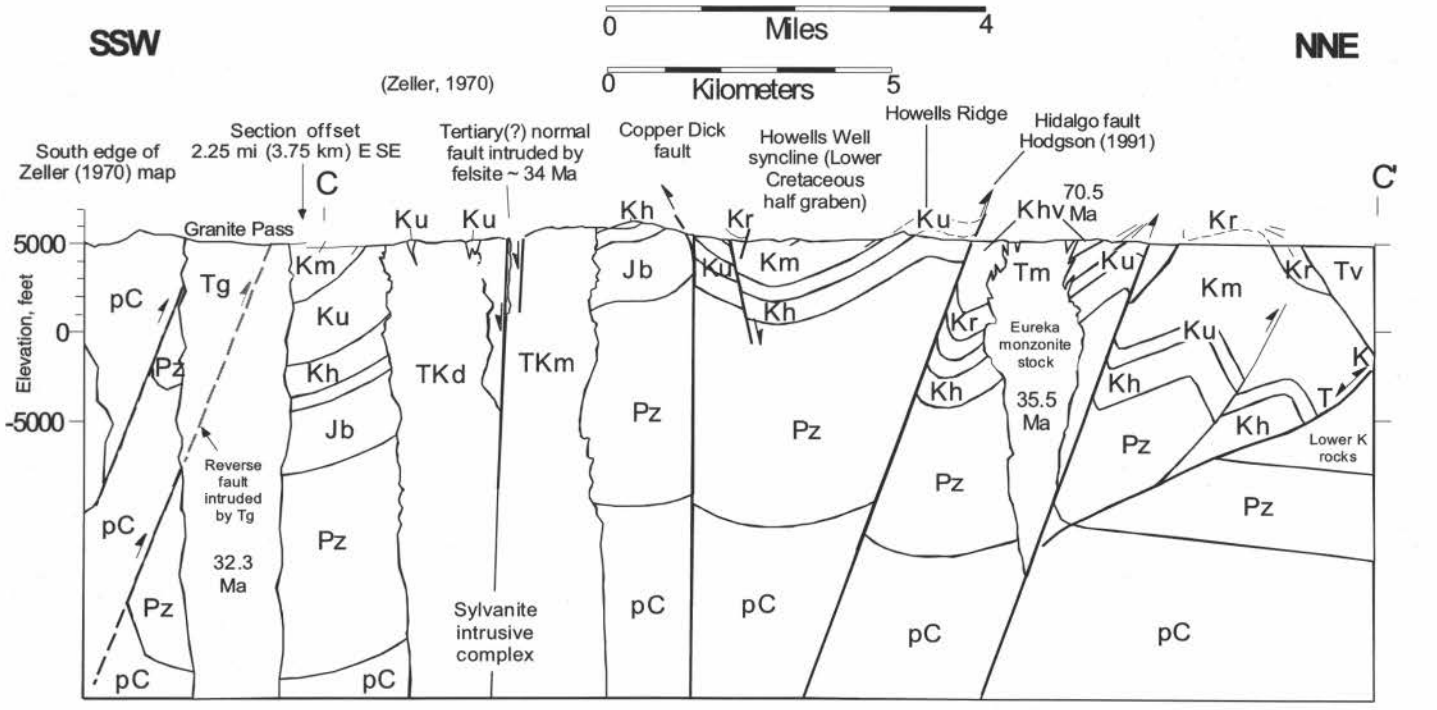


FIGURE 7. North–south cross-section through the Little Hatchet Mountains, along the lines noted on Figure 2.

ACKNOWLEDGMENTS

Partially supported by grants from the New Mexico Geological Society and the Russell and Frankie Clemons Field Scholarship. Thanks to Chris McKee, NMBMMR, for analytical work and the Research Reactor Center at the University of Missouri-Columbia for INAA determinations. Jeff Amato and Elizabeth Anthony, whose comments are appreciated, reviewed an earlier version of this manuscript.

REFERENCES

Ervin, S. D., 1998, Cambrian plutonism in southern New Mexico: The Florida Mountain intrusion [M.S. thesis]: Las Cruces, New Mexico State University, 78 p.

Harrigan, P. J., 1995, Stratigraphy, depositional environments and tectonic setting of the Broken Jug Formation (Late Jurassic?–Early Cretaceous) in the Little Hatchet Mountains, southwestern New Mexico [M.S. thesis]: Las Cruces, New Mexico State University, 101 p.

Lanphere, M. A. and Dalrymple, G. B., 1976, Identification of excess ^{40}Ar by the $^{40}Ar/^{39}Ar$ age spectrum technique: Earth and Planetary Science Letters, v. 32, p. 141–148.

Lawton, T. F. and Harrigan, P. J., 1998, Jurassic Broken Jug Formation: Redefinition of lower part of Bisbee Group, Little Hatchet Mountains, Hidalgo County, New Mexico: New Mexico Geology, v. 20, p. 69–77.

Lawton, T. F. and McMillan, N. J., 1999, Arc abandonment as a cause for passive continental rifting—Comparison of the Jurassic Mexican Borderland rift and the Cenozoic Rio Grande rift: Geology, v. 27, p. 779–782.

Lawton, T. F. and Olmstead, G. A., 1995, Stratigraphy and structure of the lower part of the Bisbee Group, northeastern Chiricahua Mountains, Arizona, USA: Geological Society of America, Special Paper 301, p. 21–39.

Lovera, O. M., Richter, F. M. and Harrison, T. M., 1989, $^{40}Ar/^{39}Ar$ thermochronometry for slowly cooled samples having a distribution of diffusion domain sizes: Journal of Geophysical Research, v. 94, p. 17,971–17,935.

McDougall, I. and Harrison, T. M., 1999, Geochronology and thermochronology by the $^{40}Ar/^{39}Ar$ Method: Oxford University Press, New York, 269 p.

Thompson, R. N., 1982, Magmatism of the British Tertiary volcanic province: Scottish Journal of Geology, v. 18, p. 49–107.

Wasson, J. T., 1985, Meteorites: their record of early solar-system history: W. H. Freeman, New York, 267 p.

Zeller, R. A., 1965, Stratigraphy of the Big Hatchet Mountains area, New Mexico: New Mexico Bureau of Mines and Mineral Resources, Memoir 16, 128 p.

Zeller, R. A., 1970, Geology of the Little Hatchet Mountains, Grant and Hidalgo counties, New Mexico Bureau of Mines and Mineral Resources, Bulletin 96, 22 p.